Geophys. J. Int. (1993) **113,** 284–298

Polar wandering of a dynamic earth

Yanick Ricard,[1] Giorgio Spada[1,2] and Roberto Sabadini[2]
[1] *Département de Géologie, Ecole Normale Supérieure, 24 rue Lhomond, 75231 Paris Cedex 05, France*
[2] *Dipartimento di Fisica, Settore Geofisica, Università di Bologna, Viale Berti Pichat 8, 40127 Bologna, Italy*

Accepted 1992 September 2. Received 1992 August 7; in original form 1992 April 6

SUMMARY

The rotational behaviour of a stratified visco-elastic planet submitted to changes in its inertia tensor is studied in a viscous quasi-fluid approximation. This approximation allows for large displacements of the Earth rotation axis with respect to the entire mantle but is only valid for mass redistribution within the planet occurring on the time scale of a few million years. Such a motion, called true polar wander (TPW), is detected by palaeomagneticiens assuming that the Earth's magnetic field remains on average aligned with the spin axis. Our model shows that a downgoing cold slab induces a TPW which quickly brings this slab to the pole for a mantle of uniform viscosity. The same slab is slowly moved toward the equator when a large viscosity increase with depth takes place in the mantle. Our model is also suitable to investigate the effects of a non-steady-state convection on the Earth's rotation. We discuss these effects using a simple mass redistribution model inspired by the pioneering paper of Goldreich & Toomre (1969). It consists of studying the TPW induced by a random distribution of slabs sinking into the mantle. For such a mass redistribution, only a strongly stratified mantle can reduce the Earth's pole velocity below $1°\,Ma^{-1}$, which is the upper bound value observed by palaeomagnetic investigations for the last 200 Ma. Our model also shows that when corrected for the hydrostatic flattening, the Earth's polar inertia generally corresponds to the maximum inertia, as it is presently observed. However, this may not be the case during some short time periods. We also discuss the amount of excess polar flattening that can be related to tidal deceleration. This frozen component is found to be negligible.

Key words: geoid, mantle rheology, polar wander.

DYNAMIC EQUATION OF A DEFORMABLE ROTATING BODY

The equation of motion of a rotating body in a rotating frame is the well known Euler dynamic equation. When no external torque is applied, it reads

$$\frac{d}{dt}(J\cdot\omega)+\omega\wedge J\cdot\omega=0. \qquad (1)$$

where J is the second-order symmetric inertia tensor and ω is the angular velocity. Both are expressed in a rotating Earth-fixed coordinate system. This equation also holds when J is a time-dependent function (Munk & MacDonald 1960). In this case, it takes the name of Liouville equation.

The inertia tensor J is traditionally divided into three contributions of decreasing amplitudes. The first is the tensor of a spherical non-rotating Earth. We write it as $I\delta_{ij}$ where δ_{ij} is the Kronecker symbol. This term is close to $0.33\,Ma^2$ where M and a are the mass and the radius of Earth. A second term is due to the centrifugal potential that deforms the Earth. It can be shown that this potential is proportional to $\omega_i\omega_j-\frac{1}{3}\omega^2\delta_{ij}$ where ω_i are the components of ω in the geographical frame (e.g. Lambeck 1980). Any change in rotation is therefore equivalent to a new potential applied to the Earth's surface. Under such a boundary condition, the planet evolves toward a new configuration corresponding to an inertia tensor equal to the convolution of $k^T(t)$, the tidal Love number of harmonic degree 2, with the time history of the changes in the centrifugal potential (Takeuchi, Saito & Kobayashi 1962). It can be shown that the contribution related to the rotation is $\frac{k^T(t)a^5}{3G}*[\omega_i(t)\omega_j(t)-\frac{1}{3}\omega^2(t)\delta_{ij}]$ where G is the gravity constant and $*$ represents the time convolution. From the previous equation it is easy to see that a planet rotating at a constant velocity Ω, reaches a steady-state axisymmetrical

shape with a polar inertia $C = I + \frac{2}{3}\frac{k_f^T a^5}{3G}\Omega^2$ and two equatorial inertia $A = I - \frac{1}{3}\frac{k_f^T a^5}{3G}\Omega^2$ where the fluid tidal Love number k_f^T is the limit of $k^T(t)$ for very large times. The I inertia is therefore equal to $(C+2A)/3$ and the amplitude of the rotational contribution to inertia is $C - A = \frac{k_f^T a^5}{3G}\Omega^2$. Assuming that the Earth is close to a perfect hydrostatic equilibrium, this last value can be identified as the observed flattening $C - A = 1.08\,10^{-3}\,\mathrm{Ma}^2$. The third and last term in the inertia tensor J is related to the mass redistribution inside the Earth or at its surface. In a general way we can write this term $[\delta(t) + k^L(t)] * C_{ij}(t)$ where $C_{ij}(t)$ represents the inertia changes due to a given geophysical process, without taking into account any dynamic deformation. These changes of inertia act directly on the planet through the $\delta(t)$ Dirac function. They may also have a delayed effect due to induced isostatic compensation. These effects are taken into consideration through the time convolution with an isostatic Love number $k^L(t)$ of harmonic degree 2, where the upperscript L stands for 'loading'. The amplitude of the $C_{ij}(t)$ terms can be computed for simple excitation sources. As an example, the Pleistocenic deglaciation corresponds to a change of inertia with an amplitude of about $10^{-5}\,\mathrm{Ma}^2$. The inertia tensor can therefore be written as

$$J_{ij}(t) = I\delta_{ij} + \frac{k^T(t)a^5}{3G} * [\omega_i(t)\omega_j(t) - \tfrac{1}{3}\omega^2(t)\delta_{ij}] + [\delta(t) + k^L(t)] * C_{ij}(t), \quad (2)$$

where the three terms of the right-hand side are of order 0.33, $1.08\ 10^{-3}$, and $1\ 10^{-5}\,\mathrm{Ma}^2$, respectively.

This equation has generally been studied under a linearized form where only the perturbations of ω close to a starting vector Ω have been taken into account. Such an approximation has been used for both short- and long-term processes. On a time scale of a few thousand years, eqs (1) and (2) have successfully modelled the changes of rotation due to the last deglaciation (Sabadini & Peltier 1981; Wu & Peltier 1984; Lefftz & Legros 1992). On a time scale of a few million years, the same equations have been used to estimate the effects of mantle convection on polar wander (Sabadini & Yuen 1989; Ricard & Sabadini 1990; Ricard, Sabadini & Spada 1992). The general non-linear problem governed by eqs (1) and (2) has only been solved for very simple models and for constant excitation sources (Munk & MacDonald 1960; Lefftz 1991).

The goal of this paper is to study the effects of a time-dependent mantle mass redistribution for the Earth's rotation. We are only interested in slow varying processes that could induce a TPW velocity comparable to the observed value of around $1°\,\mathrm{Ma}^{-1}$ and that could eventually move the Earth's pole by a large amount. Our practical problem is to compute realistic Love numbers and to efficiently perform the convolutions appearing in eq. (2).

LONG-TERM BEHAVIOUR OF LOVE NUMBER

A radially stratified visco-elastic planet has a set of deformation eigen modes characterized by their patterns and their relaxation times τ_i or inverse relaxation times $s_i = -1/\tau_i$ (Peltier 1974; James 1991; Spada 1992). As an example, a simple homogeneous viscoelastic sphere deforms through a single mode $M0$ (Munk & MacDonald 1960). A purely viscous mantle surrounding an inviscid core has two modes, $M0$ and $C0$. These two modes correspond to symmetrical and antisymmetrical deformations of the surface and of the core–mantle boundary, respectively (Richards & Hager 1984). A more complex stratified Earth leads to a larger set of modes. Some of them have characteristic times close to the Maxwell times of each visco-elastic layer (T transient modes). The lithospheric mode $L0$ is related to the presence of an elastic lithosphere. The $M0$, $C0$ and $L0$ modes have characteristic times of about one thousand years. In addition to these, some very slow modes ($M_1, M_2, \ldots$) are associated with the return to the equilibrium of non-adiabatic density interfaces within the mantle. $M1$ corresponds to the possible non-adiabatic density jump at 670 km depth and $M2$ to another density jump within the upper mantle. These modes only relax after a few million years.

The time dependence of Love numbers for a given harmonic degree is generally expressed through their Laplace transform. Their general form is (Peltier 1974):

$$k(s) = k_e + \sum_{i=1}^{M} \frac{k_i}{s - s_i}. \quad (3)$$

In this equation, the number of modes M depends on the model density stratification and on the presence of a lithosphere. The residue k_e takes into account the instantaneous elastic deformation while the k_i are associated with each visco-elastic mode. The convolution of this response with a Heaviside excitation leads to a time domain response of the form:

$$k(t) = k_e - \sum_{i=1}^{M} \frac{k_i}{s_i}(1 - e^{s_i t}). \quad (4)$$

The $k(s)$ and $k(t)$ functions can be computed for a surface tidal forcing or for a loading acting at the surface or inside the Earth (Takeuchi *et al.* 1962; Hinderer, Legros & Crossley 1991; Spada 1992). Different k_e and k_i correspond to these different cases, but the relaxation times remain the same. For an internal loading problem, k_e and k_i depend on the source depth.

As seen from the previous equations, the numerical difficulty of solving the non-linear problem arises from the fact that different time scales spanning various decades are interacting. These time constants are ranging from zero (the elastic impulse) to the relaxation time of several million years associated with the $M1$ mode. The geophysical excitations also have a very large time span. This forbids any direct approach to the integro-differential system expressed by eqs (1), (2) and (4). The complexity of numerical integration is further increased by the fact that $\omega(t)$ is never monotonously varying but is revolving at a Chandler period of about 435 days around an average solution.

We must therefore derive an approximate solution of these equations. In this paper we are only interested in very slow geophysical processes such as plate motions or mantle convection. In that case, our excitation function only varies with time constants larger than say 1 Ma. Let us first assume

that our Earth model has no internal non-adiabatic density gradients (no $M1$ or $M2$ modes) so that its largest relaxation time is much smaller than 1 Ma. In this hypothesis, $|s_i t| \gg 1$ or equivalently $|s| \ll |s_i|$ and we can easily approximate eqs (3) and (4). For the loading case, our approximation leads to

$$k^L(s) = k_e^L - \sum_{i=1}^{M} \frac{k_i^L}{s_i}. \tag{5}$$

We can therefore identify the time-dependent isostatic Love number $k^L(t)$ with its fluid limit k_f^L. For the tidal case the approximation is somewhat more complex. We must allow for the possibility of a time-dependent flattening in order to account for the effects of the readjustment of the equatorial bulge during polar wander. To do this, we keep an s term in the Taylor expansion of $k^T(s)$ (Munk & MacDonald 1960). Therefore, $k^T(s)$ can be approximated to the first order by

$$k^T(s) = k_f^T(1 - T_1 s), \tag{6}$$

where the tidal fluid Love number k_f^T is defined, similarly to the loading fluid Love number k_f^L in eq. (5), as

$$k_f^T = k_e^T - \sum_{i=1}^{M} \frac{k_i^T}{s_i}, \tag{7}$$

and where the time constant T_1 is

$$T_1 = \frac{1}{k_f^T} \sum_{i=1}^{M} \frac{k_i^T}{s_i^2}. \tag{8}$$

Numerically the k_e^T and k_i^T are found positive so that T_1 is also positive. In the case without internal non-adiabatic density jumps, our approximations are very good as the relaxation times are at least two orders of magnitude smaller than the time characterizing the variations in $C_{ij}(t)$ considered in this paper.

What happens if the mantle has internal non-adiabatic density jumps? The Taylor expansion of (3) is still valid for $|s| \ll |s_{M1}|$, which means that our approximation holds for geophysical processes slower than the relaxation time $-1/s_{M1}$ that controls the readjustment of the 670 km depth chemical discontinuity. The quality of the approximation (6) is reinforced by the fact that, for most of the realistic models of the Earth's mantle, the amplitude of k_{M1}^T is negligible. In other words, this vanishing k_{M1}^T strength means that a change in the Earth's centrifugal potential does not induce any appreciable displacement of the 670 km depth interface. For the loading problem, the role of the $M1$ mode can be more important. When $k^L(s)$ is computed for masses located inside the mantle, the amplitude k_{M1}^T associated with the $M1$ mode, can be large. In this case, we separate the slowest mode and substitute the following equation for (4),

$$k^L(t) = k_f^L + \frac{k_{M1}^L}{s_{M1}} e^{s_{M1} t}. \tag{9}$$

This equation that expresses the convolution of the loading Love number with a Heaviside function, assumes that for the time scale under consideration, all the modes, except possibly the $M1$ mode, have already relaxed. The convolution between the exponential part of $k^L(t)$ and $C_{ij}(t)$ is numerically performed without any problem even with a large time step as both terms are varying very slowly with time.

In Figs 1 and 2 the Love numbers are respectively depicted in the Laplace domain for a tidal boundary condition and for an internal loading problem where the load is located at 670 km depth. Our Earth model consists of a viscoelastic upper mantle ($\eta_1 = 10^{21}$ Pa s^{-1}, $\mu_1 = 1.5\,10^{11}$ Pa), a viscoelastic lower mantle 10 times more viscous ($\eta_2 = 10^{22}$ Pa s^{-1}, $\mu_2 = 2.5\,10^{11}$ Pa) and an inviscid core. A 100 km thick purely elastic lithosphere ($\mu_L = 4.0\,10^{10}$ Pa, $\rho_L = 2900$ kg m^{-3}) is present in the computations depicted in the right column of each Figure. The whole mantle has a density equal to $\rho = 4500$ kg m^{-3} in the upper rows. The mantle density increases at 670 km depth, from $\rho_1 = 4300$ kg m^{-3} to $\rho_2 = 4800$ kg m^{-3} in the bottom rows. The computed Love numbers expressed by eq. (3) are depicted with a thick line. The various singularities correspond to the modes $T1$, $T2$, $M0$ and $C0$ for the model with uniform mantle (1a and 2a). The $L0$ mode shows up in cases (1b and 2b). Cases in panels (c) and (d) differ from (a) and (b) by the presence of the slow $M1$ mode.

A dotted line is used to represent our approximations deduced from eq. (6) for the tidal Love number (Fig. 1) and from eqs (5) (Figs 2a and 2b) or (9) (Figs 2c and 2d) for the loading problem. For short times, the dotted lines do not fit the discontinuities associated with the various poles. In the time range under interest (more than a few Ma), our approximations precisely match the exact functions. In the case of a chemically stratified Earth submitted to a tidal boundary condition (Figs 1c and 1d), the $M1$ mode is active in such a narrow s interval ($k_{M1}^T \simeq 0$) that it can be neglected. On the contrary, for loading problems (Figs 2c and 2d), the $M1$ mode is strongly excited and is taken into account by our approximation.

In the limit of very long times, the tidal Love numbers reach asymptotically their fluid values. These limits are independent from the viscosities. They are related to the density profiles and somewhat to the presence of an elastic lithosphere in which some stress can be frozen even after a long time. The fluid values range from $k_f^T = 1.00$ for density stratified models with lithosphere to $k_f^T = 1.05$ for models with uniform mantle density. They closely match the real value deduced from the Earth's flattening $k_f^T = 0.94$. For very short times, the elastic tidal Love numbers k_e^T computed from our models are ranging from 0.28 to 0.30, and give a very good fit with the observed value deduced from the Earth's body tides $k_e^T = 0.29$ (e.g. Lambeck 1980).

The time T_1 used in eq. (6) is depicted in Fig. 3 as a function of the ratio between lower and upper mantle viscosities in the case without (a) or with lithosphere (b). Here, a reference upper mantle viscosity has been chosen equal to 10^{21} Pa s. A multiplication of this reference viscosity by a given factor approximately changes T_1 by the same factor. The time T_1 is increasing with the viscosity ratio and is always of the order of 1–10 k yr. This slowing down is imposed by a simple physical mechanism. The viscosity increase inhibits the mantle circulation and confines the flow to the upper mantle low-viscosity channel. The time T_1 is not very sensitive to the nature of the 670 km depth interface (Sabadini & Yuen 1989).

The values of $1 + k_f^L$ deduced from our models are shown in Fig. 4 as a function of the depth of the exciting source.

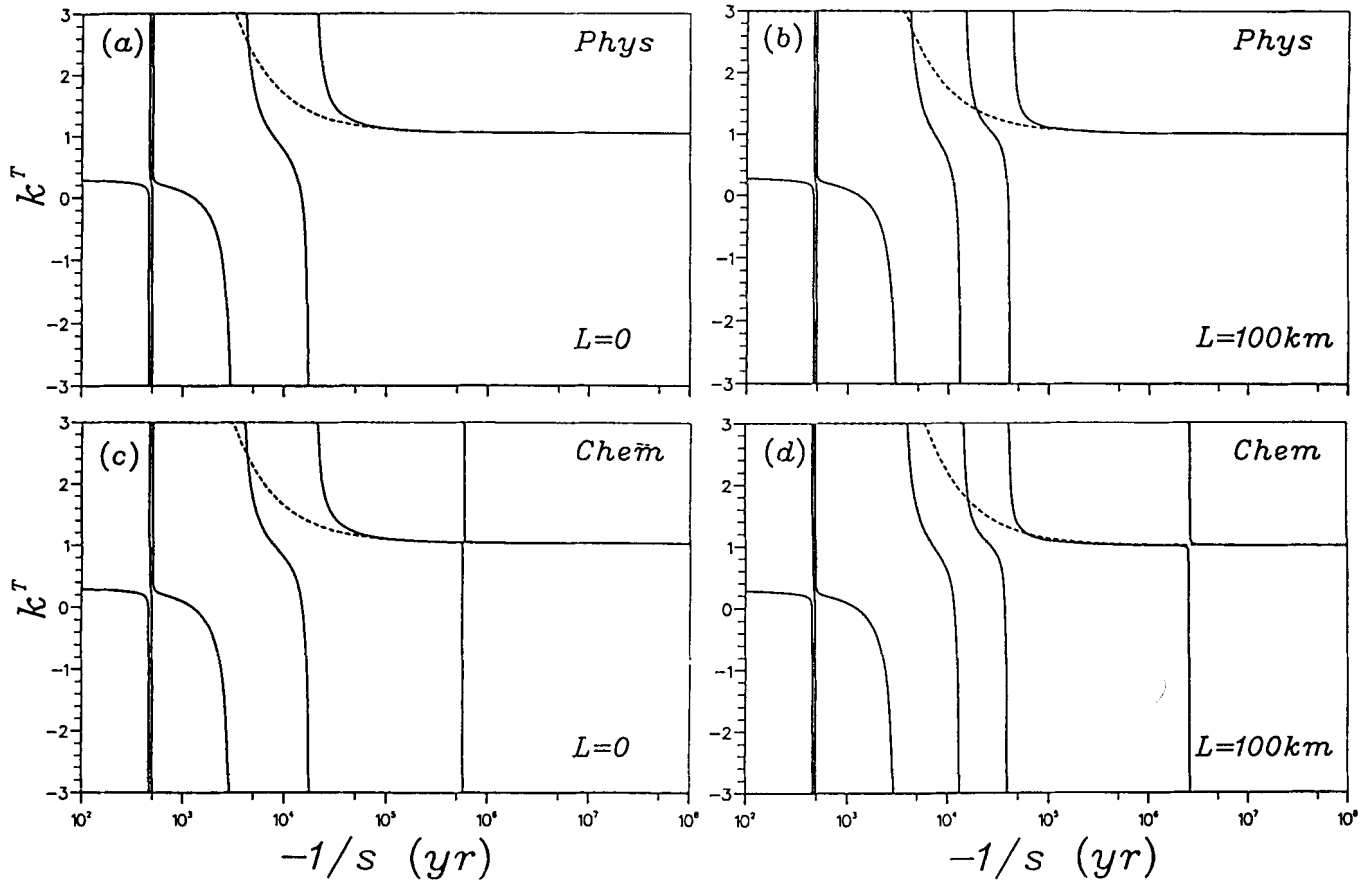

Figure 1. Tidal Love number of degree 2 as a function of the Laplace variable s. The Love numbers are plotted by a full line. The discontinuities correspond to the different visco-elastic modes. For all cases the lower mantle viscosity is 10 times larger than the upper mantle one. In (a), the Earth model has a uniform density and the modes $T1$, $T2$, $M0$ and $C0$ are present. The existence of an elastic lithosphere in (b) induces the presence of an additional $L0$ mode. The slow $M1$ mode induced by a possible non-adiabatic density jump at 670 km depth is seen in the bottom row (c and d). Our Love number approximations (dashed lines) are valid for slow time-varying processes.

For mass anomalies close to the core–mantle boundary these functions are zero. In the case of non-adiabatically stratified models (bottom row), the mass anomalies are also perfectly compensated when they lay close to the 670 km depth density jump. For masses at the surface, $1 + k_f^L$ is also zero in the case without lithosphere (left column). A slight undercompensation is supported by elastic stresses when the lithosphere is present (right column). For moderate viscosity increases in the mantle, a positive mass anomaly gives rise to a negative $1 + k_f^L$. Larger viscosity variations can impose a positive $1 + k_f^L$ on top of the same positive mass anomaly.

The inertia tensor is related to the geoid of degree 2. The excitation functions $1 + k_f^L$ only differ from the geoid kernels (Ricard, Fleitout & Froidevaux 1984; Richards & Hager 1984) by a normalization function. We have verified that the long term limits of our viscoelastic models without purely elastic lithospheres reproduce exactly what has been obtained for purely viscous steady-state models. The equivalence between long-term viscoelastic models and viscous steady-state models needs some clarification. This means that when $t \to \infty$ or $s \to 0$, our viscoelastic model assumes the character of a Newtonian viscous fluid (Wu & Peltier 1982; Wu 1992) and has the same surface Love numbers. For internal loads, the displacements inside the viscoelastic mantle tend to infinity when $s \to 0$ but the associated velocities approach finite values equal to those found for steady-state viscous models. The viscous limit of a viscoelastic model obtained when $s \to 0$ cannot be directly found by assuming $s = 0$ in the rheological law. This would correspond to the rheology of an inviscid fluid. The fact that steady-state viscous models can be used even though the loads are moving is justified because the boundary deformations are generally rapid compared to changes in the position of the loads. However, eq. (9) allows us to take into account the upper–lower mantle interface that readjusts slowly.

The need for keeping the M1 mode in the convolution of the load history with the isostatic Love numbers is illustrated in Fig. 5. For four chemically stratified models, we computed the time dependent excitation function $1 + k^L$. In the top row of Fig. 5, the mantle viscosity is uniform whereas it increases by a factor 50 in the lower row. The right column differs from the left one by the presence of a lithosphere. The Love numbers deduced from eq. (4) are plotted by a dashed line, 0.2 Ma (panel a) or 1 Ma (panels b, c and d) after the imposition of a Heaviside load. At that time, the Love numbers are far from reaching their asymptotic values (full lines). Hence the necessity of using eq. (9) instead of eq. (5) when chemically stratified models are used.

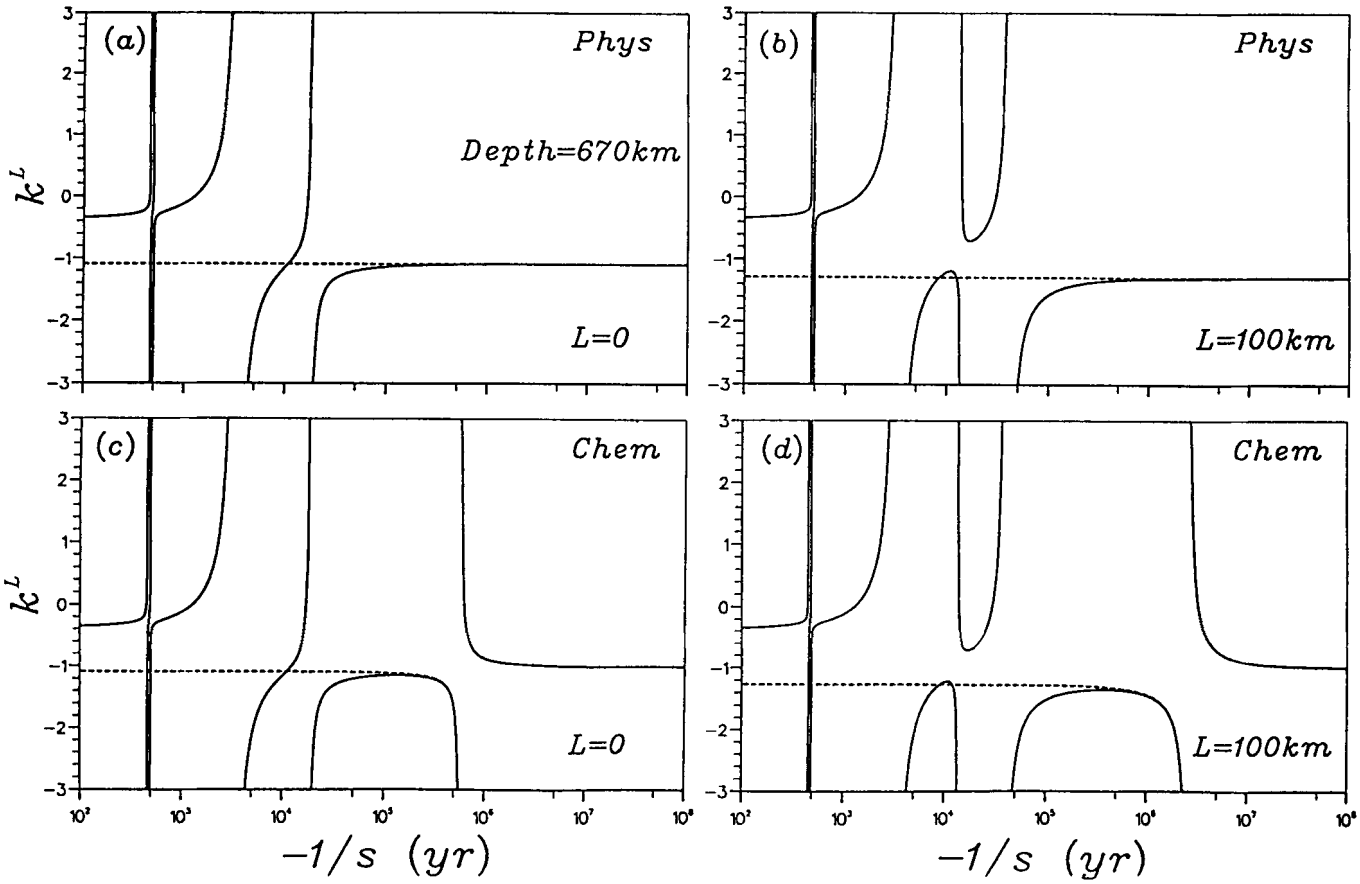

Figure 2. Same as Fig. 1 but for isostatic Love numbers. The loading Love numbers have been computed for a mass anomaly located at the upper–lower mantle interface. The importance of the $M1$ mode is clearly seen on panels (c) and (d). In the bottom row, the loading Love numbers asymptotically reach the value -1 when s tends to zero. This corresponds to a perfect local isostatic compensation.

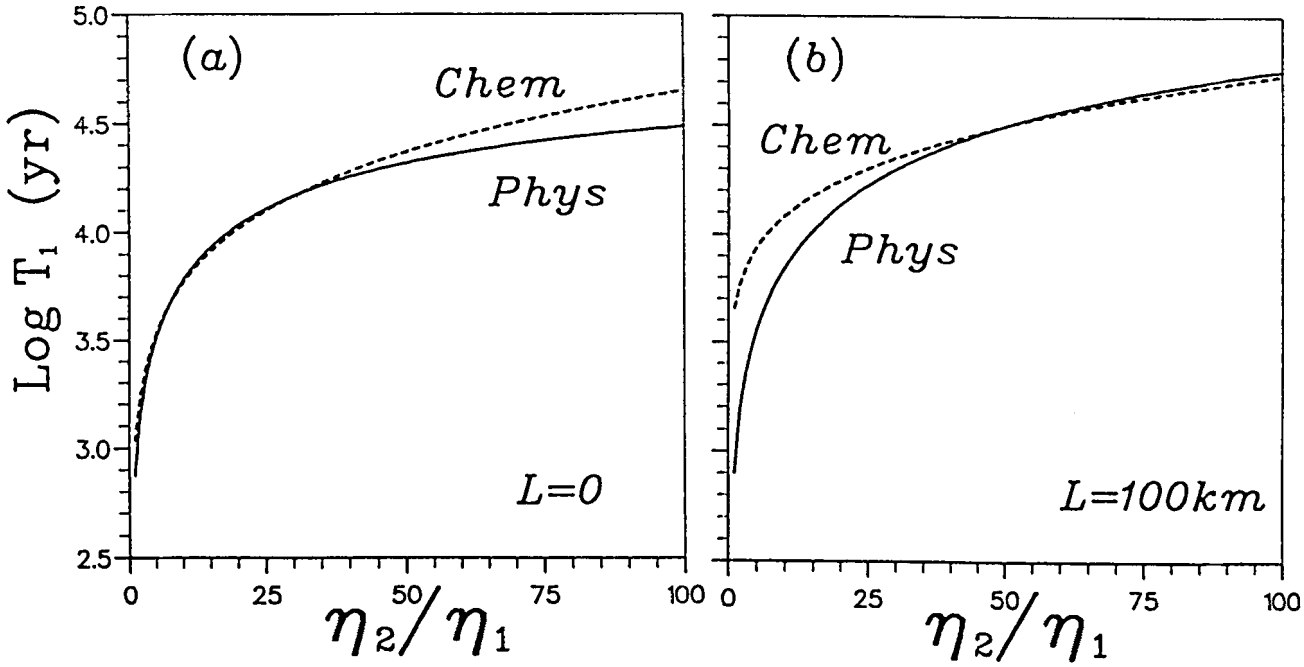

Figure 3. Characteristic time T_1 defined from eq. (8) as a function of the viscosity ratio between upper and lower mantle. The upper mantle viscosity is kept at $\eta_1 = 10^{21}$ Pa s. The full line corresponds to a mantle of uniform density. The dotted line is obtained for a lower mantle 9 per cent denser than the upper one. The time T_1 is not very sensitive to the mantle density stratification.

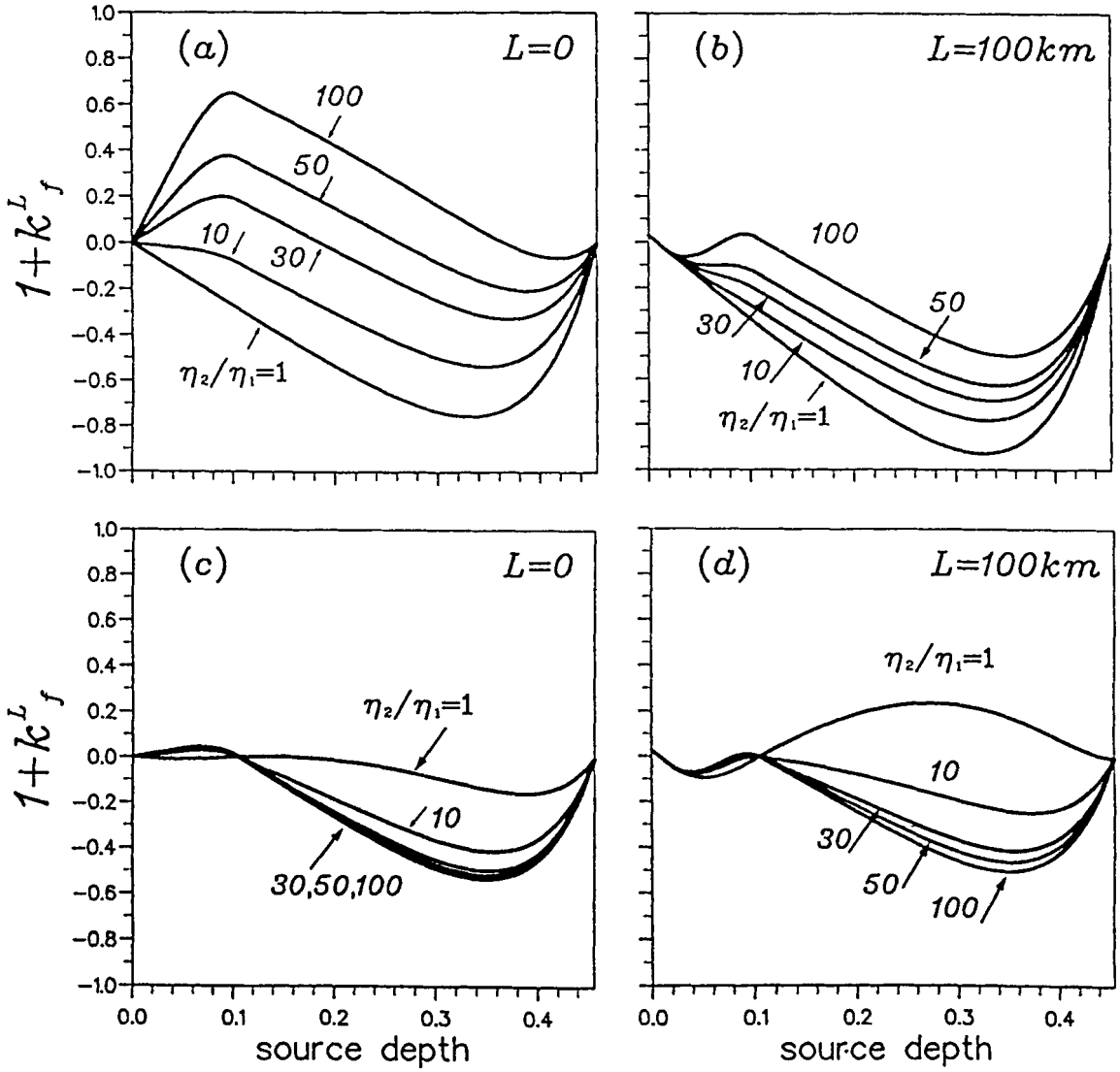

Figure 4. Inertia perturbation in the long-term approximation due to an inertia source of unit amplitude introduced at time $t = 0$ in the mantle. This perturbation $1 + k_f^L$, is plotted as a function of the mass anomaly depth for a viscosity jump at the upper–lower mantle interface by a factor 1, 10, 30, 50 or 100. In the first row, the mantle density is uniform, in the second row it increases by 9 per cent at 670 km depth. A lithosphere is present in the right column.

LONG-TERM POLAR WANDER

We can now use the eqs (6) and (9) to derive a new expression of eq. (2). Taking into account the fact that the Laplace transform of a convolution is a product and that the Laplace image of a time derivative $\dot{f}(t)$, is $sf(s)$, eq. (2) reads

$$J_{ij} = I\delta_{ij} + \frac{k_f^T a^5}{3G}(\omega_i\omega_j - \tfrac{1}{3}\omega^2\delta_{ij}) - \frac{k_f^T a^5}{3G}T_1(\dot{\omega}_i\omega_j + \omega_i\dot{\omega}_j - \tfrac{2}{3}\omega_l\dot{\omega}_l\delta_{ij}) + E_{ij}, \tag{10}$$

where the time dependence is implicit and where E_{ij} is obtained by convolving $C_{ij}(t)$ with $\delta(t) + k^L(t)$. We have seen that this last convolution can be simply approximated by $(1 + k_f^L)C_{ij}(t)$ for Earth models without internal density jumps. For chemically stratified models, the convolution is performed numerically.

From eqs (1) and (10), neglecting the terms in $\ddot{\omega}$ and $\dot{\omega}^2$ for consistency with our approximation (6), we get

$$A_{ij}(\omega)\dot{\omega}_j + B_{ij}(\omega, E, \dot{E})\omega_j = 0, \tag{11}$$

where

$$A = \frac{k_f^T T_1 a^5}{3G}\begin{pmatrix} \frac{3GI}{k_f^T a^5 T_1} & \omega^2\omega_3 & -\omega^2\omega_2 \\ -\omega^2\omega_3 & \frac{3GI}{k_f^T a^5 T_1} & \omega^2\omega_1 \\ \omega^2\omega_2 & -\omega^2\omega_1 & \frac{3GI}{k_f^T a^5 T_1} \end{pmatrix}, \tag{12}$$

$$B = \begin{pmatrix} \dot{E}_{11} & \Sigma_3 & -\Sigma_2 \\ -\Sigma_3 & \dot{E}_{22} & \Sigma_1 \\ \Sigma_2 & -\Sigma_1 & E_{33} \end{pmatrix}, \tag{13}$$

and

$$\Sigma_k = E_{ki}\omega_i. \tag{14}$$

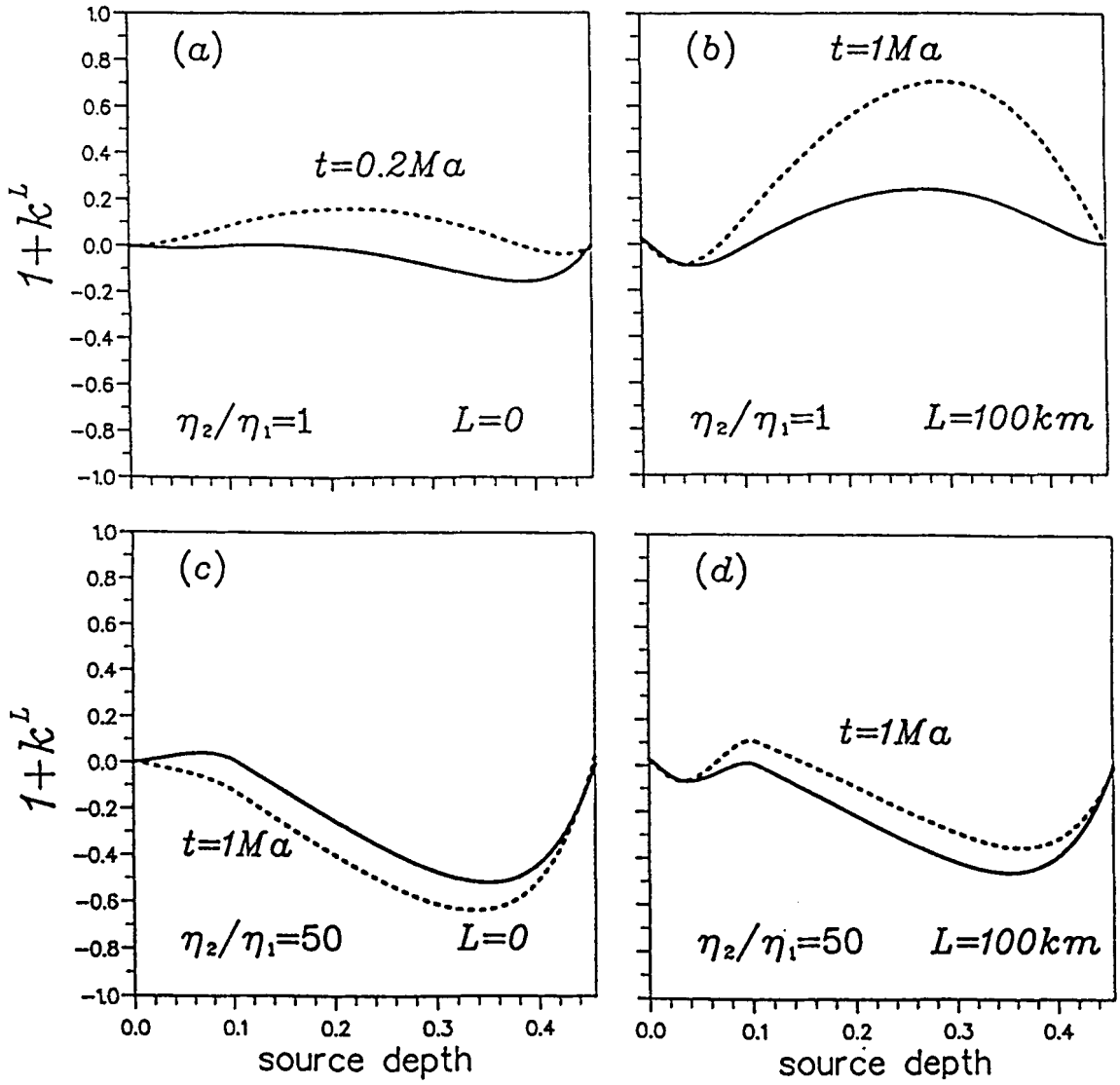

Figure 5. Inertia perturbation $1 + k^L$ computed at time $t = 0.2$ Ma or $t = 1$ Ma after the introduction of a mass anomaly (dashed line). A full line depicts the fluid limit obtained at very long time. The models used in the four panels are stratified in density and the long-term behaviour is controlled by the $M1$ mode. On top, the mantle viscosity is uniform, on bottom it increases by a factor 50. A lithosphere is present in the right column. For cases (b), (c) and (d) the asymptotic regime is only reached after millions of years.

As the diagonal terms of A are smaller than the non-diagonal terms, a further approximation could be to neglect them (Lefftz 1991). In that case, A is not inversible, and the conservation of ω^2 must be imposed. This last approximation could have been directly deduced from (1). In effect, it corresponds to totally neglecting the $J\,d/dt$ in front of $J \cdot \omega$ as the changes in long-term polar motion occur on a much longer time scale than the diurnal Earth rotation. However, we have seen that the inertia tensor J includes terms of very different relative amplitudes, spanning five decades, so that the largest term in $J\,d/dt$ which is $I\,d/dt$, is only 10^{-3} of the smallest term in $J \cdot \omega$ which is $\frac{k_f^T T_1 a^5 \omega^2}{3G}\omega$. Even including its diagonal terms, the matrix A is not too numerically ill-conditioned. Although somewhat extreme, the approximation consisting in neglecting the diagonal terms helps to understand the basic physics of polar wander on long term scale. This approximation is equivalent to replacing (1) by

$$J \cdot \omega = \alpha\omega, \tag{15}$$

where α is unknown. The Euler equation degenerates into an eigenvalue problem: the angular momentum, $J \cdot \omega$ remains constantly parallel to the angular velocity ω. Equivalently, eq. (15) indicates that, the non-diagonal terms of J, J_{zx} and J_{zy}, in a reference frame where z coincides with ω, are zero in the long-term approximation. The reader must be aware, of course, that the J inertia matrix includes not only the effects of internal masses in a dynamic non-rotating Earth, but also the rotational deformations. The main inertia of the exciting source C_{ij} is not necessarily parallel to the rotation axis.

To check the validity of our equations, we can compute the change in the rotation vector $(0, 0, \Omega)$ when perturbed at time $t = 0$ by a change in inertia. Taking into account that

$\frac{k_f^T a^5 \omega^2}{3G} = C - A$, we obtain from eqs (11) to (14)

$$\dot{\omega}_1 + i\dot{\omega}_2 = \Omega\left[\frac{1}{T_1 + iI/\Omega/(C-A)}\right]\frac{E_{13} + iE_{23}}{C-A} \tag{16}$$

$$\dot{\omega}_3 = -\Omega\frac{\dot{E}_{33}}{I} \tag{17}$$

where $i = \sqrt{-1}$ is the imaginary unit. The polar motion and the change in the length of day are respectively governed by eqs (16) and (17). As shown by previous studies, the two problems appear to be decoupled for short time scales (e.g. Lambeck 1980). Eq. (17) is identical to what is obtained by linear theories. Our eq. (16), deduced from a quasi-fluid approximation, can be derived by the approximation at large times of the results obtained by Sabadini, Yuen & Boschi (1984) from the linear theory. The quantity inside square brackets in eq. (16) is exactly what they called the rotational steady-state residue A_1.

Equation (16) can help us to better understand the differences between the inertia tensor of the non-rotating dynamic Earth E_{ij} and the rotating dynamic Earth J_{ij}. The observed present-day polar wander has a velocity of $1°\,\mathrm{Ma}^{-1}$ and is directed toward the Hudson Bay. It is mainly related to post-glacial rebound (Sabadini & Peltier 1981). Although the elapsed time since the deglaciation is too short for a complete relaxation of the modes entering in the tidal relaxation process, we can use eq. (16) to estimate an order of magnitude of the excitation presently driving the pole. For $T_1 = 20$ k yr which corresponds to a viscosity increase in the mantle by around 25 (see Fig. 3), the requested excitation $E/(C-A)$ amounts to $3.5\,10^{-4}$, a value which can be translated in terms of a geoid anomaly of degree 2 and order 1 of about 7 m. The tensor E of the non-rotating Earth presents non-diagonal terms E_{zx} and E_{zy} associated with a 7 m high geoid anomaly of degree 2 and order 1, whereas the tensor J of the rotating Earth is purely axisymmetrical and associated with a geoid without terms of degree 2 and order 1. The very existence of the tensor E only arises from the observation of polar wander.

From (16) we see that the planet, submitted to a change of inertia of order E, will wander with a characteristic time of order $T_1(C-A)/E$. A lower bound for this time scale can be estimated from the ratio of the Earth flattening ($\simeq$21 km) to the geoid height anomalies of degree 2 ($\simeq$100 m). This characteristic time is thus larger than 200 T_1. In other words, under a change of inertia, the Earth can shift its rotation pole from a starting position to a new position in a time scale larger than a few 100 k yr or a few 1 Ma, depending upon its internal stratification.

The resolution of (11) is numerically performed by a simple fourth-order Runge–Kutta algorithm. It generalizes for a stratified Earth and a complex load history the solution obtained by Milankovitch (1934) in a discussion of possible polar wander induced by the distribution of continents on top of a homogeneous viscoelastic Earth.

The validity of our approximations has also been checked by comparison with a hybrid treatment of the non-linear Liouville equations (Spada 1992). This method, inspired by a scheme provided in Sabadini & Peltier (1981), consists of keeping separate the slowest relaxation mode also in the tidal part, by analogy with what we did for only the loading part (see eq. 9). The simple differential system (11) with three equations is replaced by a new set of nine equations which are solved by a Runge–Kutta method with a time-step lower than the characteristic $M1$ time. This approach gives us a better approximation of $k^T(s)$ than our eq. (6). The agreement between the two methods is excellent, confirming the negligible role of the $M1$ mode in the tidal response of the Earth.

SOME REMARKS ON POLAR WANDERING

The title of this paragraph is taken from the title of a famous paper on polar wander written by Goldreich & Toomre (1969). Their paper is supporting the idea that continental drift is able to drive large displacements of the Earth's pole. Their simple model consists in a quasi-rigid sphere roamed by a colony of N beetles. Such animals had been introduced for geophysical purposes by Gold (1955) a few years before. Goldreich & Toomre assume that the equatorial bulge follows the rotation axis instantaneously and that no free wobble is excited. Their main point is that for large N the speed of polar motion exceeds by a factor $\sqrt{N}$ the average speed of the beetles.

The Goldreich & Toomre quasi-rigid model has, in fact, both k^L and k^T equal to zero. Of course, the Earth differs from such a simple model. First, the bulge follows the rotation only after a delayed time related to the mantle viscosity ($T_1 \neq 0$). Second, the isostasy tends to cancel the inertia anomaly associated with every Gold's beetle. We have seen that surface loads, and in a general way all loads located close to an interface, are not driving any polar motion in our long term approximation, as $1 + k^L(t)$ tends to zero as t increases. For the Earth, the only way to drive long-term polar motion is therefore with mantle circulation. The efficient mass anomalies are not crawling at the surface but sinking inside.

We first chose to mimic the effect of a slab located at 45° from the north pole. The slab has a mass of 2×10^{19} kg. This corresponds to a slab pull of $5 \times 10^{13}\,\mathrm{N\,m}^{-1}$ per unit length along a trench (Turcotte & Schubert 1982) having a total length of 4×10^3 km. This mass anomaly is comparable to the mass of the ice sheets melted during the last deglaciation. The effect of such loads on the speed of polar wander is known to be about $1°\,\mathrm{Ma}^{-1}$ (Sabadini & Peltier 1981). Of course, since this surface loading has driven and will drive polar motion for only a few thousand years, the cumulative pole displacement due to Pleistocenic deglaciation will be less than 0.1°. The slab begins to act at time $t = 10$ Ma and its depth location 200, 670 or 1200 km is not evolving through time. The upper mantle viscosity is kept constant ($\eta_1 = 10^{21}$ Pa s) and five different lower mantle viscosities are considered ($\eta_2 = 1$, 10, 30, 50, 100×10^{21} Pa s). The results obtained for our models with and without density jump at 670 km depth are respectively depicted on Figs 6 and 7. We only considered models without lithosphere.

Since both the time constant T_1 and the excitation function $1 + k^L$ are functions of the mantle viscosity, two effects are interacting. For a viscosity contrast lower than around 30, the polar wander brings the slab and the rotation axis closer, wherever the slabs are located within the mantle.

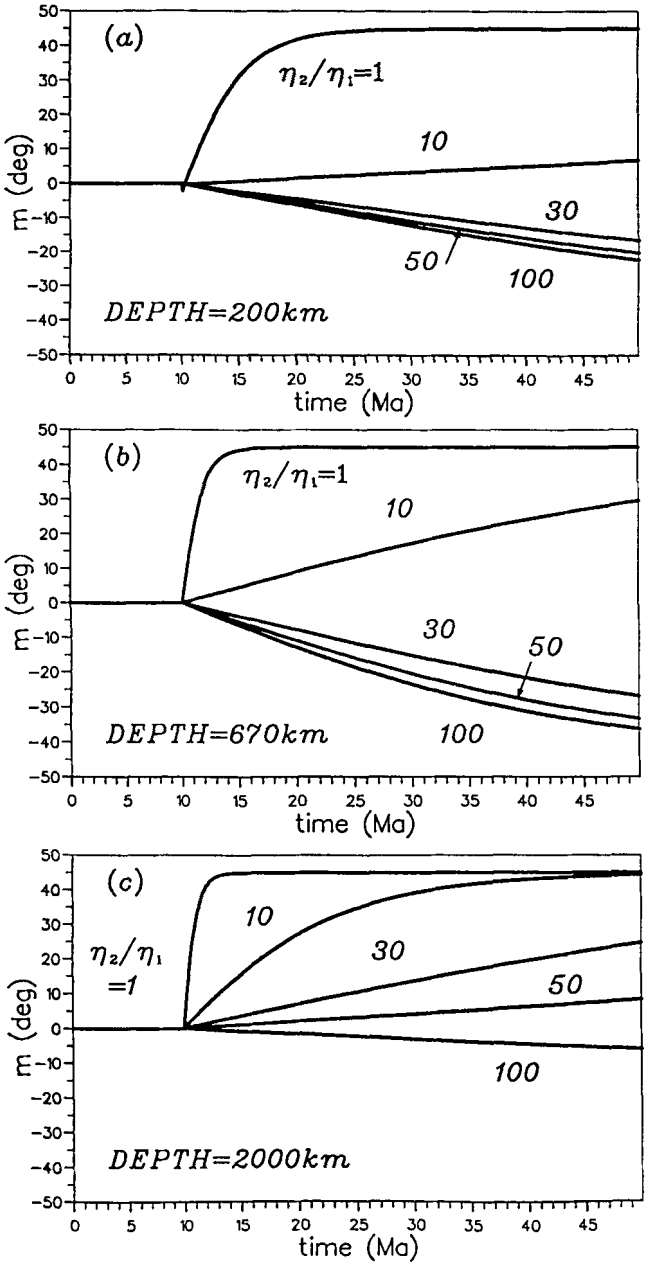

Figure 6. Polar wander in degrees induced by a dense mass of amplitude 2. 10^{19} kg introduced in the mantle at time $t = 10$ Ma. The mantle has a constant density and no lithosphere. The mass is located at 200, 670 or 2000 km depth. A positive polar wander corresponds to a pole wandering toward the mass anomaly. This is the case for moderate lower mantle viscosities.

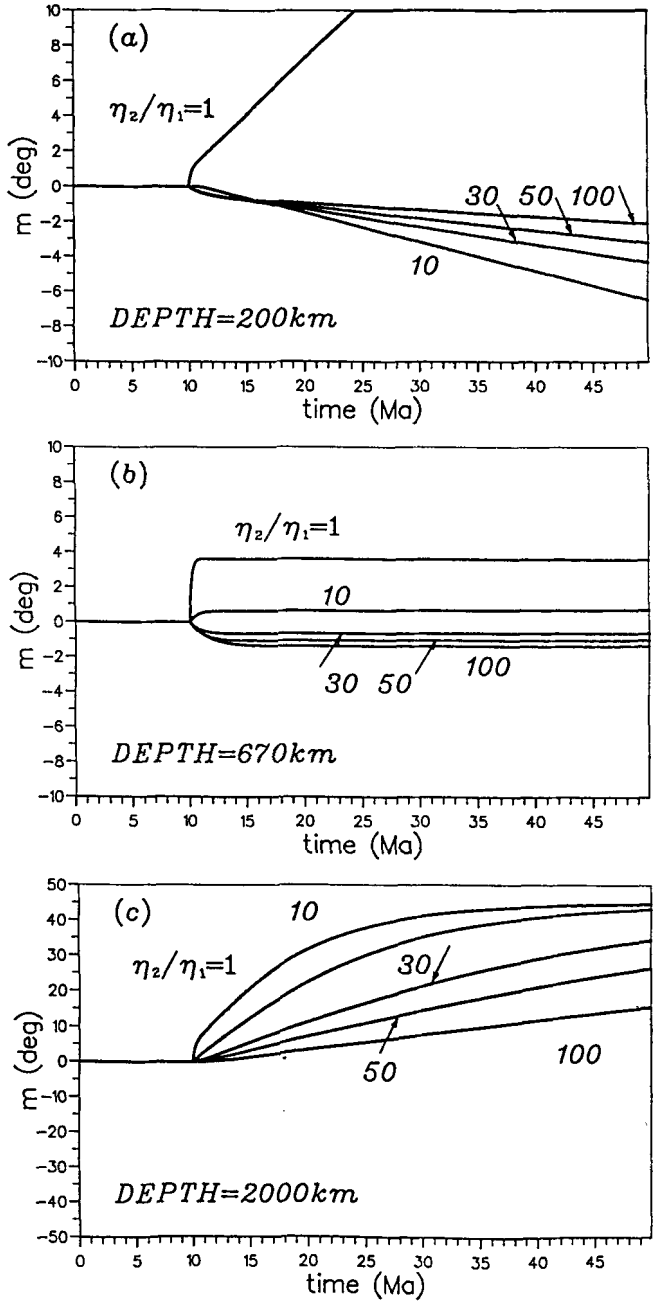

Figure 7. Same as Fig. 6 but for a non-adiabatically stratified mantle.

For a viscosity contrast larger than 30, upper mantle slabs are rejected toward the equator. Below the 670 km depth discontinuity, they are rejected toward the pole. This result is related to the change already seen in the geoid sign associated with a given mass anomaly according to its depth location and to the viscosity increase through the mantle. Of course, whatever is the polar path excited by a load at 45°, it will reach asymtotically an angular displacement equal to ±45°.

An increase in the lower mantle viscosity strongly decreases the rate of polar wander. For an adiabatically stratified mantle (Fig. 6), the polar velocity is larger than for the chemically stratified models (Fig. 7). Notice that, for upper mantle mass anomaly, we use a different scale in panels (a) and (b) of Fig. 7. In Fig. 7(b), for a mass anomaly located at the upper–lower mantle interface, the polar shift only occurs during the relaxation of the $M1$ mode. In contrast to the Goldreich & Toomre quasi-rigid approximation, where the polar displacement instantaneously occurs, our viscous quasi-fluid model needs at least a few million years to readjust even in the fastest case obtained for a uniform mantle viscosity.

We will now simulate the effect of a downwelling slab or more precisely a cold blob as our mass anomaly is not

connected to the surface. The blob begins to sink in the mantle at time $t = 10$ Ma with a velocity of 10 cm yr^{-1}. It has the same mass 2 10^{19} kg, as in the previous numerical experiments. This velocity is supposed to be constant throughout the mantle so that the mantle is crossed after 30 Ma. The computations have been performed both with a phase change and a chemical interface at the upper–lower mantle interface. Of course, in models with a chemical interface, the slab itself cannot physically cross the interface. We simply assume that a mass anomaly is induced by thermal coupling through the interface. For simplicity, this new cold blob is also sinking at a velocity of 10 cm yr^{-1}. The results are depicted in Fig. 8. The four panels correspond to our four rheological models, in the top row the mantle is physically stratified, while in the bottom row we assume a non-adiabatic density jump at 670 km depth. The right panels differ from the left ones by the presence of a lithosphere.

As the excitation term, proportional to $1 + k^L$, is equal to zero at the surface, the polar displacement has a zero time derivative when the slab begins to sink. For modest viscosity increases by a factor 1 or 10, the polar wander is toward the slab, except for a chemically stratified homogeneous mantle with a lithosphere (panel d). For larger viscosity increases, the pole can oscillate, as is seen in panel (a). While the blob is crossing the upper mantle, the pole moves away from it. Then, as the blob goes down in the lower mantle, the excitation function changes sign and forces the slab and the pole to move closer together. In a physically stratified mantle without lithosphere, the pole returns to its starting position at a viscosity increase of around 30. A slab velocity following a Stokes law would have been reduced in the highly viscous lower mantle. This would have given the pole a longer time to move farther from the slab and then, also a longer time to return closer to its starting position.

We now want to present an idealized model for mass redistribution within the mantle in order to show the potential effect of convection on the rotation of the Earth. Of course, we could have taken a computation of 3-D convection to estimate the order of magnitude of changes in the inertial terms $C_{ij}(t)$ entering in eq. (2). We have chosen to use a simple model that catches some of the basic features of mantle convection and is inspired by the Goldreich & Toomre paper. We assume that slabs randomly distributed on the sphere, the analogues of the Gold's beetles, are falling inside the mantle. Every two million years a new slab is sinking. Their velocity in the upper mantle is equal to 10 cm yr^{-1} and is reduced accordingly to the increase in mantle viscosity in the lower mantle. On average, eight blobs are present at the same time in the upper mantle.

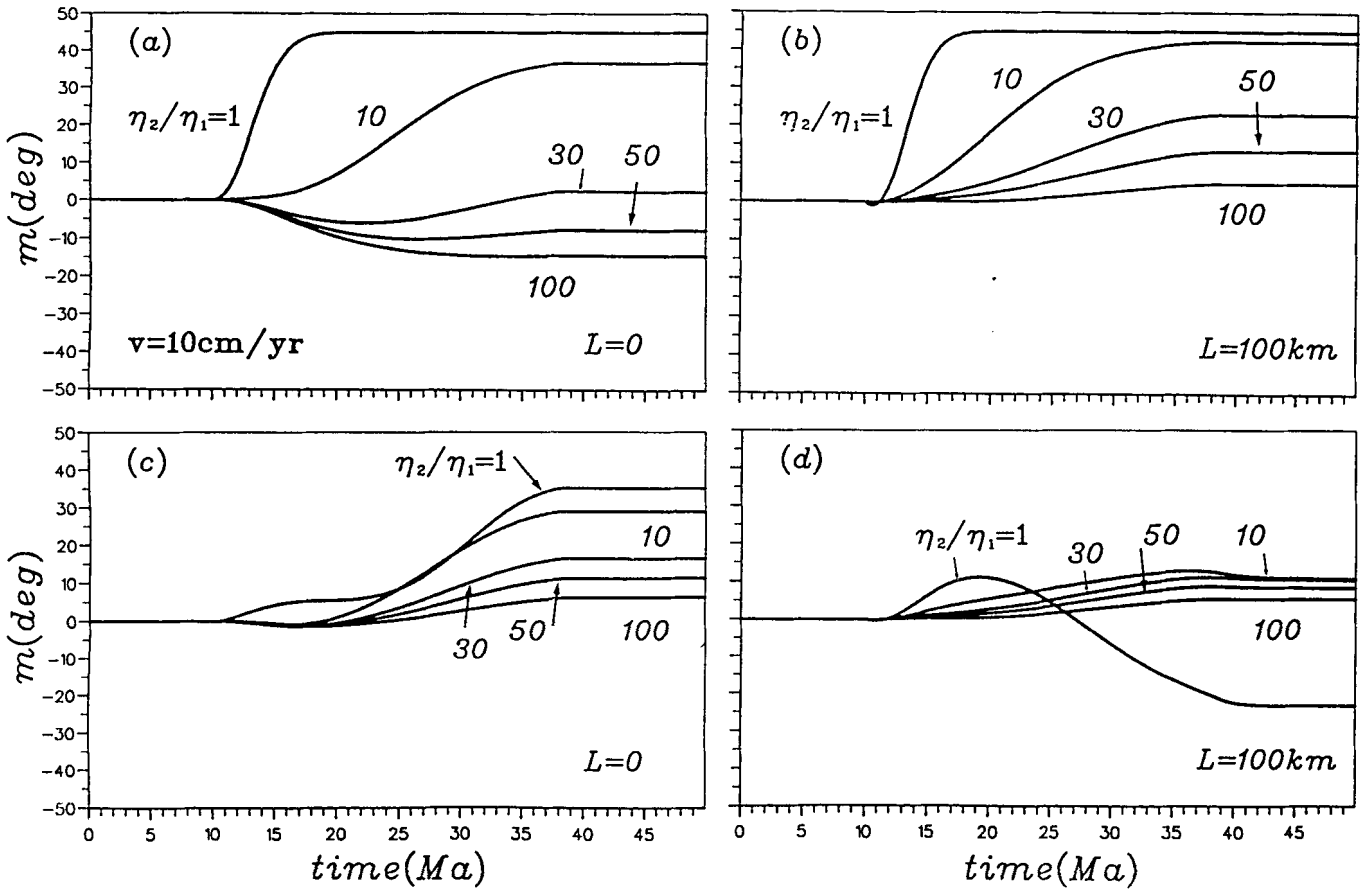

Figure 8. Polar motion induced by a downgoing slab beginning to sink in the mantle at time $t = 10$ Ma. In the top row the mantle is adiabatically stratified, a density jump of 9 per cent is present in the bottom row. The lithosphere is present in the right column. The lower mantle viscosity is 1, 10, 30, 50 or 100 times larger than that of the upper mantle. The polar-wander velocity can change sign during the descent of the cold blob.

They all have the same mass of $2 \cdot 10^{19}$ kg. From this naive mantle convection we computed the inertia tensor of our model Earth in a constant geographical frame for a time span of 500 Ma. We subtract one third of its trace, from the diagonal elements of this tensor, so that the average inertia tensor of the Earth is not evolving with time. Otherwise, our slabs constantly bringing new dense material to the centre of the planet, would increase the rotation of the Earth by decreasing its inertia. This phenomenon has indeed occurred during the accretion of the core but its study is beyond the scope of the present paper.

The results of our computations are depicted in Fig. 9 (a and b), for two different rheological stratifications. Our Earth model is adiabatically stratified in both cases. In 9(a), the mantle is uniform, whereas the lower mantle viscosity is increased by a factor 30 in 9(b). The bottom part of each panel depicts the variations of the three components of the rotation vector in a geographical frame. The velocity

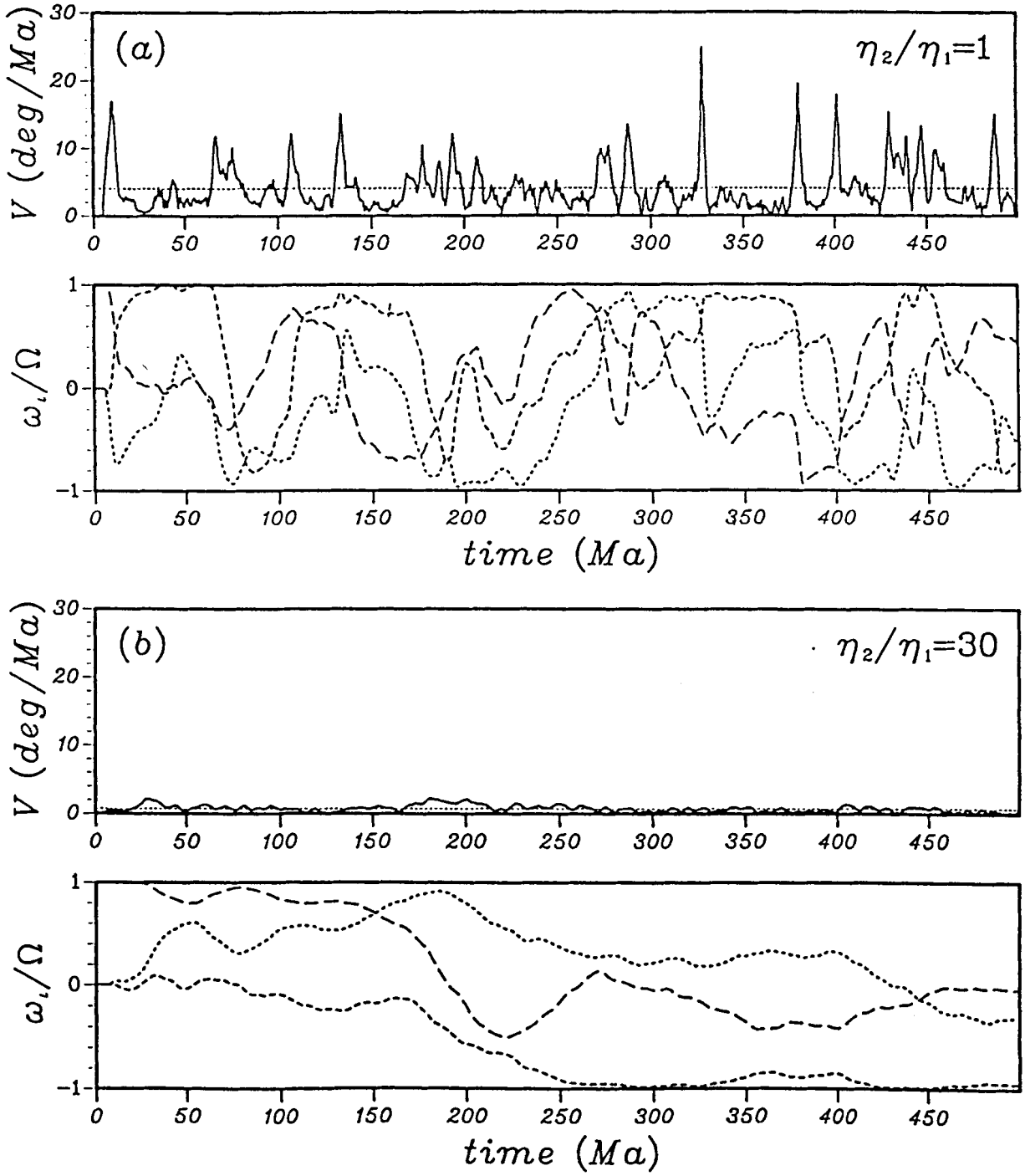

Figure 9. Velocity of polar wander and normalized components of the angular velocity vector in an Earth-fixed reference frame induced by a random distribution of sinking slabs. In panel (a) the mantle is uniform and the Earth rotation axis is highly unstable. A viscosity increase by a factor 30 in the lower mantle (b) drastically reduces the amplitude of TPW rate. The 670 km depth interface is supposed to be a phase-change discontinuity.

components have been normalized by the amplitude of the initial rotation vector. The top part of each panel shows the rate of TPW in $°Ma^{-1}$. The average TPW velocity is depicted by a dashed line.

The differences between the rotational behaviour of a uniform and a stratified mantle are striking. A viscosity increase at 670 km depth inhibits the mantle flow and slows down the average TPW velocity below $1°\,Ma^{-1}$. This slowing down is due to three concurrent effects. First, the viscosity jump decreases the slab velocities and thus, the amplitudes of the time derivatives of the inertia tensor. Second, it decreases the amplitude of the loading excitation term $1 + k_f^L$ at least for a viscosity increase lower than 100 (see Fig. 4). Third, it increases the time T_1 of the rotational response by channeling the flow into the upper mantle.

In the model with a homogeneous mantle, each slab is crossing the whole mantle in about 30 Ma so that after a transient regime of 30 Ma, our model reaches a steady-state behaviour where the slabs are uniformly distributed in the mantle. As we assume a Stokes law for the slab velocity, the steady-state regime of the model with a 30 times more viscous lower mantle is not attained in Fig. 9(b). The TPW is, in fact, somewhat further decreased in the steady-state regime as the slowly varying heterogeneities of the lower mantle stabilize the planet.

In Fig. 10, we compute the average TPW velocities induced by a random distribution of sinking slabs for different lower mantle viscosity. In the left panel the 670 km depth interface is a phase transition, while in the right panel we assume a non-adiabatic density jump. As we already supposed, the sinking blobs are nevertheless crossing this interface. The small dots are obtained using Love numbers computed for model Earth with a 100 km thick lithosphere; no lithosphere is present in the computations depicted by the large dots. The slight increase in average velocity obtained by the adiabatic model without lithosphere for large lower mantle viscosities is related to the large values reached by the excitation function (see Fig. 4).

As we used a random distribution of slabs, other results could have been obtained with other distributions, but the main conclusions we can draw from Fig. 10 would not have changed. The lower mantle viscosity has at least to be increased by a factor 5 with respect to the upper mantle one to reduce the TPW velocity below $1°\,Ma^{-1}$ which is a conservative upper bound for the observed TPW in the last 200 Ma (Besse & Courtillot 1991). For a more acceptable average TPW velocity of $0.5°\,Ma^{-1}$, the required viscosity increase is one order of magnitude.

THE EXTRA FLATTENING OF THE EARTH

Due to its rotation, the Earth is deformed with a polar flattening of about 21 km. On the one hand, from space observations, the gravity potential of degree 2 and therefore the inertia tensor of the Earth has been obtained. On the other hand, the hydrostatic flattening of our planet can be computed from the radially symmetrical models of the Earth's density deduced from seismology (Nakiboglu & Lambeck 1982). The difference between the observed and the hydrostatic inertia of the Earth leads to the non-hydrostatic tensor, related to the well known non-hydrostatic geoid of degree 2. The fact that the Earth has an

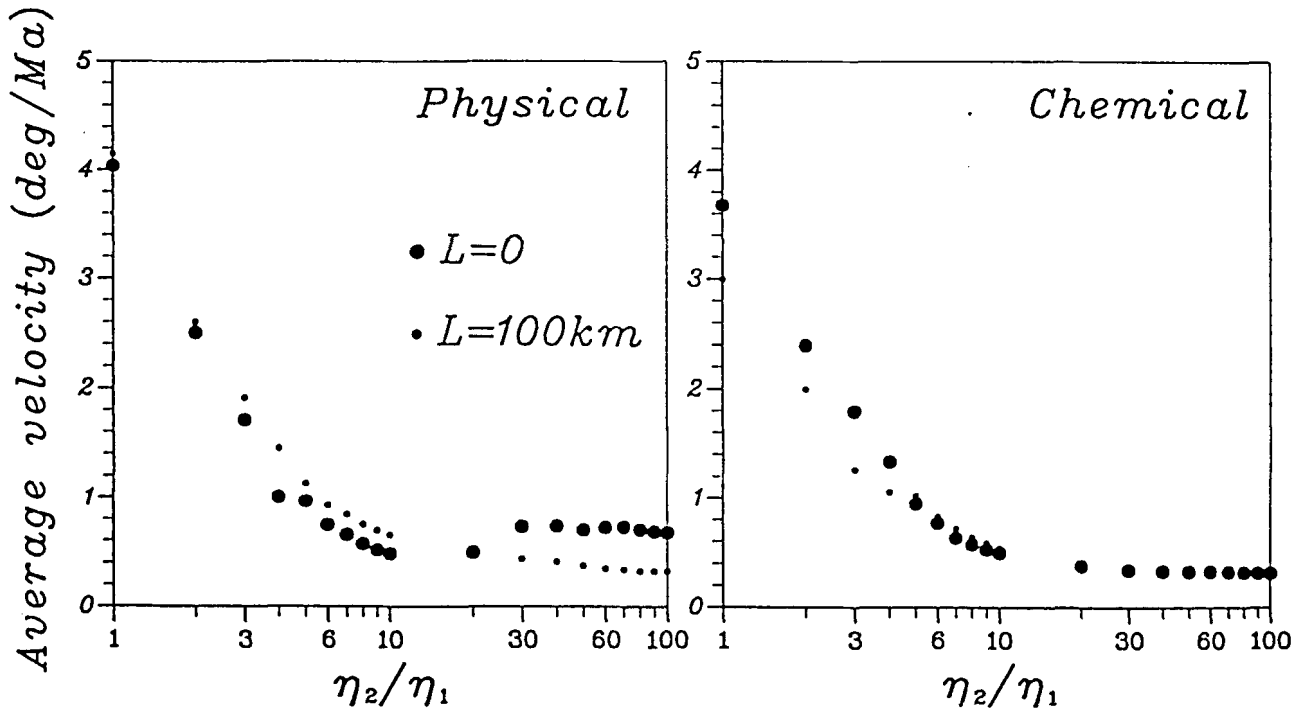

Figure 10. Rate of polar wander as a function of the lower mantle viscosity for different mantle stratifications. In the left panel, a phase-change discontinuity is assumed at 670 km depth, while in the right one a non-adiabatic density jump is present. The small dots depict the solutions obtained in the presence of an elastic lithosphere. As the excitation sources are randomly generated, somewhat different results may be obtained. According to palaeomagnetic evidence, an upper bound for the TPW velocity in the last 200 Ma is around 0.5–1° Ma. This is only obtained for models having a viscosity increase with depth larger than a factor 10.

excess oblateness, in other words a non-hydrostatic polar inertia larger than the equatorial inertia, has been thought to warrant special explanation. A first explanation suggested that this was the result of a frozen or delayed rotational bulge, a fossil from the time when the earth turned faster (McKenzie 1966). Later, Goldreich & Toomre (1969), showed that this hypothesis was not justified as the difference between the main and the middle inertia was the same as the difference between the middle and the smallest. The polar inertia exhibits nothing remarkable except that it corresponds to the largest residual inertia.

The extra flattening is simply the difference between the observed and the hydrostatic flattening one. After normalization by Ma^2, where M is the Earth mass, it reads:

$$\Delta J_2 = \frac{C-A}{Ma^2} - \frac{k_f^T a^3 \Omega^2}{3GM}. \tag{18}$$

The observed excess inertia $\Delta J_2 Ma^2$ is much smaller than the difference between polar and equatorial inertia $C-A$. The ratio of these two quantities is comparable to the ratio of the non-hydrostatic geoid of degree 2 and order 0, to the Earth flattening, which is 100 m to 21 km. This is why, in previous rough estimates, we identified $C-A$ to be $\frac{k_f^T a^5}{3G}$. In terms of tidal Love numbers the difference between these two quantities is sometimes taken into account by introducing a secular Love number k_0 deduced from observation and slightly different from the theoretical k_f^T (Lambeck 1980).

Even though the long wavelength geoid including the excess oblateness is now more or less explained by mantle anomalies (e.g. Ricard & Vigny 1989), we should still estimate the amount of frozen bulge that may be associated with the tidal deceleration of the Earth. Assuming the shape of the Earth is entirely controlled by its rotation, eq. (10) reads:

$$J_{ij} = I\delta_{ij} - \frac{k_f^T a^5 \Omega^2}{9G}(1-3\delta_{i3})\left(1-2T_1\frac{\dot{\Omega}}{\Omega}\right), \tag{19}$$

where Ω is the Earth angular velocity and where $\dot{\Omega}$ is the tidal deceleration which is around $-5.5\,10^{22} s^{-2}$ (e.g. Lambeck 1980). Using eqs (18) and (19), and identifying C with J_{33} and A with J_{11} or J_{22} we obtain

$$\Delta J_2 = -2T_1 \frac{k_f^T a^3}{3GM}\dot{\Omega}\Omega. \tag{20}$$

With $T_1 = 20$ k yr, this excess inertia corresponds to an excess flattening of 20 cm. The delayed response of the Earth to its tidal deceleration is therefore negligible in view of the observed excess flattening of about 100 m. The amount of frozen bulge would have an amplitude comparable to the geoid anomaly of degree 2 and order 0 only for a 500 times more viscous average mantle or for a quasi-rigid lower mantle (McKenzie 1966).

In the framework of a quasi-rigid spherical Earth, Goldreick & Toomre have shown that the changes of residual inertia always steer the rotational axis so as to maximize the resultant polar moment of inertia. For their model, the rotation axis of the Earth is always the main inertia axis. This is not so obvious in our model as the planet viscosity is controlling the speed of reorientation of the bulge. We have seen as an example that for Earth models where the viscosity is greatly increasing with depth, a mass anomaly can induce opposite inertia perturbation in the lower mantle than in the upper mantle. When a slab is going down, its inertial perturbation changes sign. How does this affect the Earth's extra flattening?

The inertia of the Earth in a geographical frame is obtained using (2). Its component around the rotation axis is simply:

$$C = \frac{\omega \cdot J \cdot \omega}{\omega^2}, \tag{21}$$

whereas the average inertia perpendicular to ω is

$$A = \frac{T_r(J) - C}{2}, \tag{22}$$

where $T_r(J)$ is the trace of J.

Using eq. (18) we can estimate the excess flattening involved in the computations with random slabs that we already performed (see Fig. 9). The results are depicted in Fig. 11. For an adiabatically stratified mantle with uniform

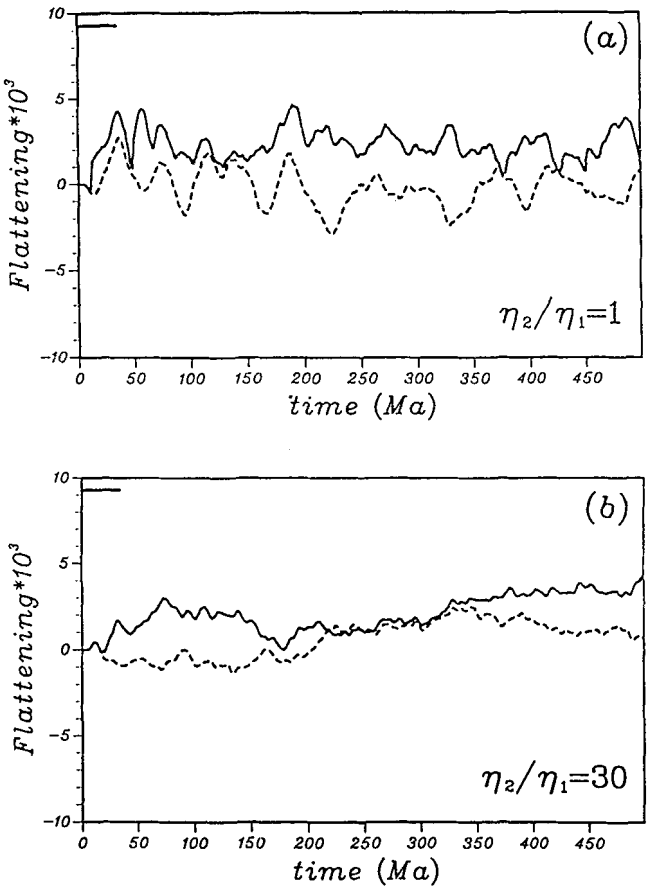

Figure 11. Flattening of our model Earth as a function of time given in Ma. The flattening is normalized by the hydrostatic Earth's flattening. It is positive for an oblate planet. This flattening has been computed in the rotational axis reference frame (full line) and in an Earth-fixed reference frame (dashed). Panel (b) differs from (a) by a 30 times more viscous lower mantle. In the rotational axis reference frame, the planet exhibits a clear average excess flattening. A thick marker indicates the present excess flattening of the Earth, $0.94\,10^{-3}$.

viscosity (a) and for an increase in viscosity by a factor 30 at 670 km depth (b), the flattening of our model in a coordinate system related to the spin axis and in an Earth-fixed coordinate system are shown with a full and a dashed line, respectively. In an Earth-fixed frame (dashed line), the randomly generated inertia tensor has a random flattening with a zero average. On the contrary, in the coordinate system orientated by the spin axis, one clearly notes the presence of an excess flattening. The values in Fig. 11 have been normalized by the hydrostatic flattening of the Earth. The value of the Earth's excess inertia in this unit $.94\,10^{-3}$, is shown by a thick marker. This value is larger than what we obtained with our over-simplified model. This probably reflects the fact that the mass anomalies in the real Earth have a lateral coherency that is not present in our slab distribution. Such a coherency imposes larger inertia anomalies than in our model.

In Fig. 11, an excess flattening is almost always observed. However, during some periods, this oblateness is very small and at the very beginning of the process the non-hydrostatic Earth undergoes a short period of prolateness. There are no mathematical reasons which prevent the non-hydrostatic Earth from spinning around an axis which is not the maximum one. One notes also that in the bottom panel, during the 200–300 Ma period, our Earth model has an over-flattening, but is not rotating around its main inertia axis as the flattening in a geographical Earth-fixed frame (dashed line) is larger.

CONCLUSIONS

Our paper reassess the physical basis of TPW induced by redistribution of masses inside the Earth that was already discussed in the book of Munk & MacDonald (1960) and in the fundamental paper of Goldreich & Toomre (1969). The main novelty arises from a realistic estimation of Love numbers for internal sources and of the time delay T_1 imposed by the mantle viscosity. Our results show that no significant amount of TPW can be induced by mass anomalies moving close to a non-adiabatic density jump. As a consequence plate motions by themselves are not the source of TPW. On the contrary, internal density heterogeneities such as downgoing slabs may be responsible for large pole displacement. Of course other sources of internal mass distribution such as those associated with non-steady-state convection or large rising plumes can excite a pole shift as well.

The viscosity and density profiles control the readjustment of the mantle reference frame with respect to the axis of rotation. Our modelling of slab penetration shows that a homogeneous mantle of viscosity 10^{21} Pa s leads to a highly unstable rotational axis. The lower mantle requires a viscosity of at least 10^{22} pa s to lower the computed rate of TPW to values observed by palaeomagneticiens. Larger lower mantle viscosities do not further reduce the TPW velocities. In model Earth with stiff lower mantle, the upper mantle sources are the main contributors to TPW.

For realistic models, the amount of polar flattening that can be related to the Earth tidal deceleration is only a few 10 cm. As the rotation axis constantly tries to follow the main inertia axis, a rotating dynamic viscous planet is generally oblate. However, the tidal memory of the Earth may force the planet to rotate for short periods around an axis which is not the main inertia axis.

ACKNOWLEDGMENTS

This work has been partly supported by the SCIENCE program of the European Economical Community N. SC1*0456 and by the INSU-DBT (Dynamique et Bilan de la Terre) program (Global Dynamics, contribution 573).

REFERENCES

Besse, J. & Courtillot, V., 1991. Revised and synthetic apparent polar wander paths of the African, Eurasian, North American and India plates, and true polar wander since 200 Ma, *J. geophys. Res.*, **96,** 4029–4050.

Gold, T., 1955. Instability of the Earth's axis of rotation, *Nature*, **175,** 526–529.

Goldreich, P. & Toomre, A., 1969. Some remarks on polar wandering, *J. geophys. Res.*, **74,** 2555–2567.

Hinderer, J., Legros, H. & Crossley, D., 1991. Global Earth dynamics and induced gravity changes, *J. geophys. Res.*, **96,** 20 257–20 265.

James, T. S., 1991. Post-glacial deformation, *PhD thesis,* University of Princeton, New Jersey.

Lambeck, K., 1980. *The Earth's variable rotation,* Cambridge University Press, Cambridge.

Lefftz, M., 1991. Aspects théoriques de la rotation de la terre et de son noyau: influence de la viscosité, *PhD thesis,* University of Strasbourg, France.

Lefftz, M. & Legros, H., 1992. Some remarks about the rotations of a viscous planet and its homogeneous liquid core: linear theory, *Geophys. J. Int.*, **108,** 705–724.

McKenzie, D. P., 1966. The viscosity of the lower mantle, *J. geophys. Res.*, **71,** 3995–4010.

Milankovitch, M., 1934. Der Mechanismus der Polverlagerungen und die daraus sich ergebenden Polbahnkurven, *Gerlands Beitr. z. Geoph.*, **42,** 70.

Munk, W. H. & MacDonald, G. J. F., 1960. *The rotation of the Earth,* Cambridge University Press, New York.

Nakiboglu, S. M. & Lambeck, K., 1982. Hydrostatic theory of the Earth and its mechanical significance, *Phys. Earth planet. Interiors*, **28,** 302–311.

Peltier, W. R., 1974. The impulse of a Maxwell Earth, *Rev. Geophys. Space Phys.*, **12,** 649-669.

Ricard, Y., Fleitout, L. & Froidevaux, C., 1984. Geoid heights and lithospheric stresses for a dynamical Earth, *Ann. Geophys.*, **2,** 267–286.

Ricard, Y. & Sabadini, R., 1990. Rotational instabilities of the Earth induced by mantle density anomalies *Geophys. Res. Lett.*, **17,** 627–630.

Ricard, Y., Sabadini, R. & Spada, G., 1992. Isostatic deformations and Polar Wander induced by redistribution of mass within the Earth, *J. geophys. Res.*, in press.

Ricard, Y. & Vigny, C., Mantle dynamics with induced plate motions, *J. geophys. Res.*, **94,** 17 543–17 559.

Richards, M. A. & Hager, B. H., 1984. Geoid anomaly in a dynamic Earth, *J. geophys. Res.*, **89,** 5987–6002.

Sabadini, R. & Peltier, W. R., 1981. Pleistocene deglaciation and the Earth's rotation: implications for mantle viscosity, *Geophys. J. R. astr. Soc.*, **66,** 553–578.

Sabadini, R. & Yuen, D. A., 1989. Mantle stratification and long-term polar wander, *Nature*, **339,** 373–375.

Sabadini, R., Yuen, D. A. & Boschi, E., 1984. A comparison of the complete and truncated versions of the Polar Wander equations, *J. geophys. Res.*, **89,** 7609–7620.

Spada, G., 1992. Rebound post-glaciale e dinamica rotazionale di un

pianeta viscoelastico stratificato, *PhD thesis*, University of Bologna, Italy.

Spada, G., Sabadini, R., Yuen, D. A. & Ricard, Y., 1992. Effects on post-glacial rebound from the hard rheology in the transition zone, *Geophys. J. Int.*, **109,** 683–700.

Takeuchi, H., Saito, M. & Kobayashi, N., 1962. Statical deformations and free oscillations of a model earth, *J. geophys. Res.*, **67,** 1141–1154.

Turcotte, D. L. & Shubert, G., 1982. *Geodynamics*, John Wiley & Sons, New York.

Wu, P., 1992. Viscoelastic versus viscous deformation and the advection of pre-stress, *Geophys. J. Int.*, **108,** 136–142.

Wu, P. & Peltier, W. R., 1982. Viscous gravitational relaxation, *Geophys. J. R. astr. Soc.*, **70,** 435–485.

Wu, P. & Peltier, W. R., 1984. Pleistocene glaciation and the earth's rotation: a new analysis, *Geophys. J. R. astr. Soc.*, **76,** 753–791.